Multiphysics Modeling of Assembly Pressure Effects on Proton Exchange Membrane Fuel Cell Performance

Y. Zhou

G. Lin

A. J. Shih

S. J. Hu[1]
e-mail: jackhu@umich.edu

Department of Mechanical Engineering,
The University of Michigan,
Ann Arbor, MI 48109-2125

The clamping pressure used in assembling a proton exchange membrane (PEM) fuel cell stack can have significant effects on the overall cell performance. The pressure causes stack deformation, particularly in the gas diffusion layer (GDL), and impacts gas mass transfer and electrical contact resistance. Existing research for analyzing the assembly pressure effects is mostly experimental. This paper develops a sequential approach to study the pressure effects by combining the mechanical and electrochemical phenomena in fuel cells. The model integrates gas mass transfer analysis based on the deformed GDL geometry and modified parameters with the microscale electrical contact resistance analysis. The modeling results reveal that higher assembly pressure increases cell resistance to gas mass transfer, causes an uneven current density distribution, and reduces electrical contact resistance. These combined effects show that as the assembly pressure increases, the PEM fuel cell power output increases first to a maximum and then decreases over a wide range of pressures. An optimum assembly pressure is observed. The model is validated against published experimental data with good agreements. This study provides a basis for determining the assembly pressure required for optimizing PEM fuel cell performance. [DOI: 10.1115/1.3081426]

Keywords: fuel cells, assembly pressure, mass transfer resistance, electrical contact resistance

1 Introduction

Proton exchange membrane (PEM) fuel cells are recognized as a promising device for a wide variety of power applications. Among the technological challenges associated with PEM fuel cells, design, manufacturing, and assembly are considered to be the most critical issues to further reducing cost and ensuring high performance. As fuel cell manufacturing scales up, the relationship between fuel cell performance and the assembly process must be well understood. During the assembly process of a PEM fuel cell stack, the gas diffusion layer (GDL), bipolar plates (BPPs), and membrane are clamped together using mechanical devices. A proper level of clamping pressure is needed to provide adequate gas sealing, as well as to reduce contact resistances at the material interfaces. However, high pressure may overcompress the membrane and GDL, crushing their porous structures and cracking the BPP. These effects may combine to yield an optimum assembly pressure.

Several models have been developed to account for the multiphysics processes in PEM fuel cells including the gas and water mass transfers, electrochemical reaction, etc. [1–7]. Assembly pressure effects, however, were not incorporated into these models. Assembly pressure causes stack compression, with most of the compression being attributed to GDL deformation, which is critical to the performance and durability of PEM fuel cells. Lai et al. [8] investigated the compression of the membrane electrode assembly (MEA, an assembly of GDL and catalyst layers) and GDL over the channel area, where thermal expansion and swelling of the membrane can lead to buckling and separation of the membrane from the GDL. It was suggested that a higher transverse shear modulus is favored in the GDL. Lee et al. [9] studied the relationship between bolting torques used in assembling PEM fuel cell stacks and the performance. An optimum bolt torque was observed in experiments. Lee et al. [10] analyzed PEM fuel cell stack assembly pressure distribution and the compliance of a single cell using the finite-element analysis. The pressures are higher near the bolts but lower at the center of the assembled PEM fuel cell stack. It was also found that assembly pressure could significantly change the porosity of GDL. Chu et al. [11] investigated the porosity change and the results showed that a PEM fuel cell with an embedded GDL with a larger porosity, consumes a greater amount of oxygen, thus a better fuel cell can be achieved. Most recently, Ge et al. [12] designed a single PEM cell to measure GDL compression and cell performance without disassembling the cell. Experimental results showed that the fuel cell performance generally decreases with increased compression, and one should expect an optimal compression ratio, especially in the low pressure region.

Most previous research attempted to obtain the assembly pressure effects via experiments, and few efforts have been made to include the influence of assembly induced GDL deformation on gas mass transfer and contact resistance. This is also true for a number of recently published papers, with most of them being purely experimental [12–14] or partly experimental studies [15,16].

In this paper, a comprehensive finite-element-based numerical model is developed to simulate the entire process including GDL deformation, GDL property change, mass transfer process, and electrical contact resistance. GDL deformation is first modeled under different assembly pressures. Then, a PEM fuel cell mass transfer model is developed based on the deformed GDL shape and modified GDL gas transport parameters. The effects of clamping pressure on mass transfer resistance and contact resistance are

[1]Corresponding author.

Manuscript received June 6, 2007; final manuscript received August 26, 2008; published online August 11, 2009. Review conducted by Ugur Pasaogullari. Paper presented at the Fifth International Fuel Cell Science Engineering and Technology Conference (FUELCELL2007), Brooklyn, NY, June 18–20, 2007.

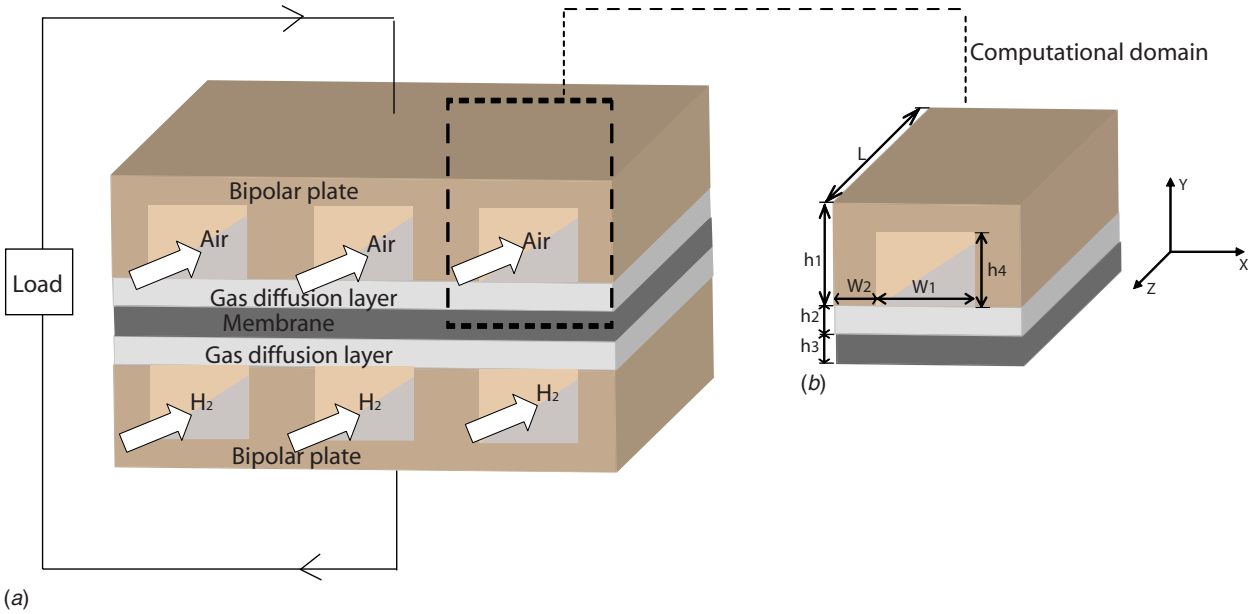

Fig. 1 Schematic of a PEM fuel cell: (*a*) cross section and (*b*) computational domain

analyzed in detail. The comprehensive fuel cell performance predicted by the model is then compared with the experimental measurements of PEM fuel cell voltage-current performance curves of Ref. [12]. Local current density and oxygen mass fraction distribution are also discussed.

2 Model Description

2.1 GDL Deformation Model. A representative 2D single-channel half-cell model for the cathode side of a PEM fuel cell is developed to study the effects of assembly pressure on the deformation of the PEM fuel cell components. Figure 1(*a*) shows the cross section of a PEM fuel cell, including the BPP, GDL, and membrane. The size of the computational domain is reduced by taking advantage of the geometrical periodicity of the cell. As shown in Fig. 1(*b*), only one channel and half of the land areas on each side need to be incorporated in the domain. Here, the *X* axis denotes the cell width direction, the *Y* axis is in the cell thickness direction, and the *Z* axis represents the cell length direction. In addition, because the length of gas channels is typically much larger (by ~2 orders of magnitude) than their cross section dimensions, which justifies the assumption of plane-strain, only a 2D model is built to reduce computational time.

The model is developed using commercial finite-element software ABAQUS. Four-node quadrilateral plane-strain elements (CPE4) are used to mesh the components with typical element sizes being 0.04×0.04 mm^2. The bottom membrane surface is fixed vertically (in *Y*-direction), and *X*-symmetry conditions are applied to the side vertical boundaries of all components. The component interfaces are bonded, with no-slip allowed. In the stack assembly, it is desirable to have a uniform assembly pressure in the BPP, even though the clamping load may be localized. As such, a uniform assembly pressure is assumed for the BPP.

The geometric and physical properties of the components are listed in Table 1. It is assumed that the effective porosity is 0.3 before compression according to Springer et al. [17] and Inoue et al. [18]. The effective porosity of GDL in the operating cell may be significantly smaller because of possible "flooding" by liquid water and compression by assembly. A series of assembly pressures from 0.04 MPa to 15 MPa are applied to the BPP top surface under which the GDL deformation is calculated. Meanwhile, the volumetric strain of every element in the GDL can be used to estimate its modified porosity. Mass transfer analysis is conducted based on the deformed configuration and the modified GDL porosity.

2.2 Mass Transfer Analysis. The same half-cell analysis domain as shown in Fig. 1(*b*) is also used in the gas mass transfer analysis. Only the overpotential on the cathode side is modeled based on the assumption that the hydrogen oxidation reaction rate is so fast that the anodic overpotential is negligible. It is assumed that the cathode is fed with humidified air: a mixture of oxygen, nitrogen, and water vapor. Steady state operation under fully-humidified conditions is assumed. The model is limited to single-phase water transport. Other assumptions used in developing the half-cell model of the gas mass transfer analysis are as follows:

(1) steady-state conditions
(2) constant cell temperature
(3) laminar flow in the fuel cell
(4) isotropic and homogenous GDL and catalyst layers
(5) ideal gas mixtures
(6) catalyst layer modeled as reactive boundaries
(7) product water in the liquid phase

Under these assumptions, a 3D model is developed to study the multicomponent flow, diffusion of reactants through the porous

Table 1 Geometric and physical parameters

Parameter	Value
Channel length (L)	20 mm
BPP thickness (h_1)	2 mm
GDL thickness (h_2)	200 μm
Membrane thickness (h_3)	50 μm
Channel height (h_4)	0.8 mm
Channel width (w_1)	1 mm
Land width (w_2)	1 mm
GDL initial porosity	0.3
Compressive modulus of BPP	10 GPa
Compressive modulus of membrane	200 MPa
GDL compressive modulus	Nonlinear elastic [19]
GDL permeability	1.76×10^{-11} m^2
Transfer coefficient for oxygen	0.5

Table 2 Binary diffusivities at reference temperatures and 1 atm [18]

Gas pair	Reference temperature	Binary diffusivities D_{ij} (m^2/s)
$D_{O_2-H_2O}$	308.1	2.82×10^{-5}
$D_{O_2-N_2}$	293.2	2.2×10^{-5}
$D_{H_2O-N_2}$	307.5	2.56×10^{-5}

GDL, and electrochemical reactions. In the BPP channel, fluid flow is modeled in combination with diffusion and convective transports. The gas flow field is obtained by solving the steady-state Navier–Strokes equations, and the pressure difference drives the flow in the channel in the following way:

$$\rho\frac{\partial u}{\partial t}-\nabla\cdot\mu(\nabla u+(\nabla u)^T)+\rho(u\cdot\nabla)u+\nabla p=0 \tag{1}$$

$$\nabla\cdot u=0 \tag{2}$$

where ρ denotes the density of the gas mixture, μ is the dynamic viscosity, p is the pressure, and u is the velocity vector.

The mass flux in the gas phase is computed based on the Maxwell–Stephan diffusion and convection equation and for the gas component i,

$$\nabla\cdot\left[-\rho\omega_i\sum_{j=1}^{N}D_{ij}\frac{M}{M_j}\left(\nabla\omega_j+\omega_j\frac{\nabla M}{M}\right)+\rho\omega_i u\right]=0 \tag{3}$$

where M is the total molar mass of the mixture, and M_j and ω_j are the molar mass and mass fraction of gas j, respectively. D_{ij} (with the unit of m^2/s) is the Maxwell–Stephan diffusivity.

The binary diffusivities D_{ij}, with its experimentally obtained values at atmospheric pressure listed in Table 2, are scaled with the temperature and pressure according to Ref. [20].

$$D_{ij}=D_{ij}(T_0,p_0)\frac{p}{p_0}\left(\frac{T}{T_0}\right)^{1.5} \tag{4}$$

In the GDL region, Darcy's law is used to model the flow through the porous media, with the pressure gradient as the driving force.

$$u=-\frac{k_p}{\mu}\nabla p \tag{5}$$

where k_p is the permeability of the GDL.

For multicomponent diffusion in the GDL, the Maxwell–Stephan equations remain the same. However, due to the porous structure of the GDL, the binary diffusivity terms D_{ij} need to be corrected for the porosity ε according to the Bruggenman correlation

$$D_{ij}^{\text{eff}}=D_{ij}\varepsilon^{1.5} \tag{6}$$

Because the catalyst layer is very thin compared with other elements within a fuel cell, it is treated as a reactive boundary. The current density distribution at the surface of the catalyst layer can be expressed as [21]

$$i_c=i_0\frac{\omega_{O_2}}{\omega_{O_{2,0}}}\exp\left(-\alpha\frac{F\eta}{RT}\right) \tag{7}$$

where i_c is the current density, i_0 represents the exchange current density of the cathode, η is the cathode activation overpotential, α is the transfer coefficient, and T is the cell operating temperature. This kinetic expression is derived from the general Butler–Volmer equation, based on the fact that the cathode has relatively slow kinetics. Because the anode exhibits fast electrokinetics, the anodic overpotential is neglected in this study. In most cases, overpotential in fuel cells refers to cathode overpotential. Hence, if only incorporating mass transfer resistance, the cell voltage is calculated as

Table 3 Operating parameters

Parameters	Value
Cathode outlet pressure	1 atm
Cathode temperature	65°C
Relative humidity of inlet fuel	100%
Inlet nitrogen/water mole faction ratio	0.79/0.21
Cathodic transfer coefficient	0.5
Dynamic viscosity μ	2×10^{-5} m^2/s
Faraday's constant	96,487
Air flow rate	2.9×10^{-4} L/s

$$E=E^0-\eta \tag{8}$$

where the open circuit potential E^0 for the overall reaction is calculated as [22]

$$E^0=0.2329+0.0025T \tag{9}$$

The electrochemical reaction at the catalyst layer determines the flux at the reactive boundary. The mass flux for consumed oxygen is

$$N_{O_2}=-M_{O_2}\frac{i_c}{4F} \tag{10}$$

where N_j represents the mass flux of gas j, and F denotes Faraday's constant.

It was assumed that the gas mixture enters at the gas flow field channel normal to the inlet cross section. All walls in the channel have no-slip boundary conditions. The mass and momentum transport boundary conditions between the BPP shoulders and the GDL are all insulated. The gas mixture enters and leaves the GDL through the boundary between the channels and the GDL. The inlet gas flow rate is calculated based on the same stoichiometric ratio as in Ref. [12]. All operating parameters are listed in Table 3.

A finite-element computational fluid dynamics package, the COMSOL Multiphysics® Chemical Engineering Module, was used to solve the fluid flow/chemical reaction equations. Using deformed geometry and parameters for each assembly pressure, the relationship between activation overpotential and current density can be obtained. Kinetic parameters for electrochemical reactions used in the simulation were adjusted in a reasonable range to fit experimental results.

2.3 Electrical Contact Resistance. Electrical contact resistance constitutes a significant part of the ohmic resistance in a fuel cell and needs to be considered when evaluating fuel cell performance. Assembly pressure affects electrical contact resistance in PEM fuel cells, with the most significant one being at the interface between the BPP and the GDL. Electrical contact resistance can be estimated based on the surface roughness parameter and features of the GDL structure. A detailed description of a recently developed contact resistance model has been published [23].

BPP surface topology is simulated as randomly distributed asperities and is based on measured surface roughness. The GDL is modeled as randomly distributed cylindrical fibers. Upon obtaining these two simulated surfaces, each contact spot is located according to their relative positions. The total resistance and pressure are obtained by considering all contact spots as resistances in parallel and summing up the results together.

Based on the analysis in Sec. 2.2, a higher assembly pressure increases the gas phase mass transfer resistance, so less assembly pressure is favored. On the other hand, the electrical contact resistance decreases with the increase in assembly pressure, meaning the ohmic overpotential can be significantly reduced. The contributions of these two effects are different in different pressure regions and can combine to yield an optimum assembly pressure.

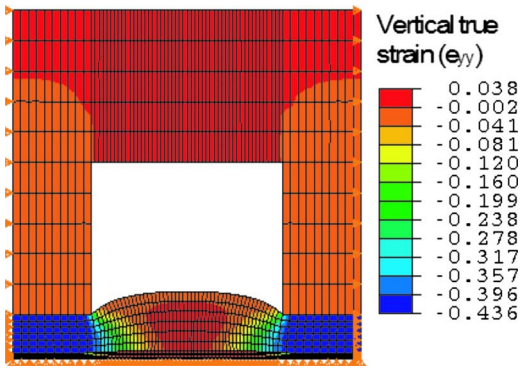

Fig. 2 Model predicted contour of effective strain at 15 MPa pressure

Consequently, to evaluate the overall performance of a PEM fuel cell, both effects need to be considered. By neglecting other bulk resistances, the cell voltage is expressed as

$$E = E^0 - \eta - \eta_{\text{contact}} \tag{11}$$

where $\eta_{\text{contact}} = 2IR_{\text{contact}}$ because of the two contacting surfaces between the BPP and the GDL in a PEM fuel cell.

3 Results and Discussions

3.1 GDL Deformation. The predicted deformation of PEM fuel cell components under a pressure of 15 MPa using the above model is shown in Fig. 2. The GDL is deformed severely, with the true strain in the Y-direction being up to 43.6%, while the BPP and membrane are nearly undeformed. Figure 3(*a*) shows the cell geometry before deformation, where $Y \in [0-0.05\ \text{mm}]$ is the membrane, and $Y \in [0.05-0.25\ \text{mm}]$ is the GDL region (0.2 mm thick). The deformed GDL shape under three different assembly pressures (0.1 MPa, 1 MPa, and 15 MPa) is illustrated in Fig. 3(*b*).

Under compression, the GDL will be compressed and deformed into the BPP channels, which affects a number of process parameters critical to the performance of PEM fuel cells. The primary effects are reduction of gas flow channel area, decrease of diffusion path under the land area, and change in porosity.

In addition to the change in GDL geometry, the porosity, which is assumed to be uniform over the whole GDL, also changed under compression. The GDL compression ratio, which is defined as the ratio of compressed thickness (under land area) to original thickness, and the porosity are shown in Fig. 4 for different assembly pressures.

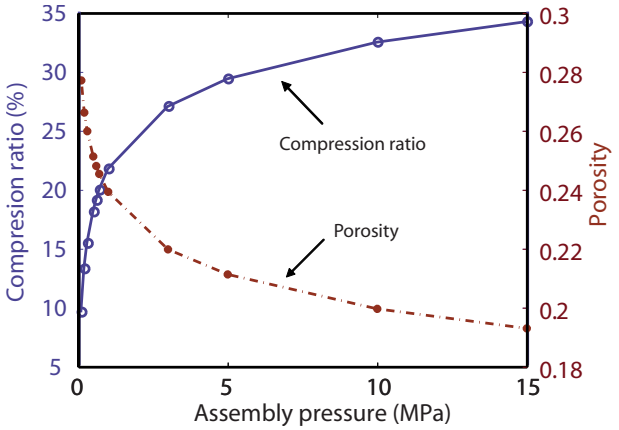

Fig. 4 Compression ratio and porosity versus assembly pressure

3.2 Assembly Pressure Effects on Mass Transfer. After assembly, the GDL is compressed and deformed into the flow channels of the BPP. As shown in Fig. 5, at the same voltage, current density is reduced at higher assembly pressure. This reflects the fact that mass transfer resistance is increased with the increase in assembly pressure. Specifically, the current density decreases by 27% when assembly pressure increases from 0.1 MPa to 15 MPa. When assembly pressure is less than 0.1 MPa, the current-voltage curve changes very slightly and stays almost the same.

This phenomenon is caused by the combined effects of flow area reduction in the channels in the BPP and a decrease in GDL thickness and porosity. The thickness and porosity of the GDL change depending on the assembly pressure. The thickness of the GDL under the land area is reduced significantly (around 36%) when the assembly pressure reaches 15 MPa. A thinner GDL indicates a shorter path for gas transportation, which could facilitate the gas transfer. At the same time, the channel flow area is reduced, and the gas velocity in the channel is increased. Both benefit gas transfer. In contrast, under compression, the porosity of the GDL decreases. It is expected that a lower porosity would impede gas transfer in the region under the land. Therefore, one effect is countered by others. To analyze these effects in detail, they are considered separately under 15 MPa assembly pressure and 0.6 V overpotential. The modeling results show that the reduction in flow area and GDL thickness could increase the generated current density by about 5%, while the decrease in GDL porosity has a more prominent effect and decreases the current density by as much as 26%. Total current density, therefore, decreases around 21% compared with nondeformed case.

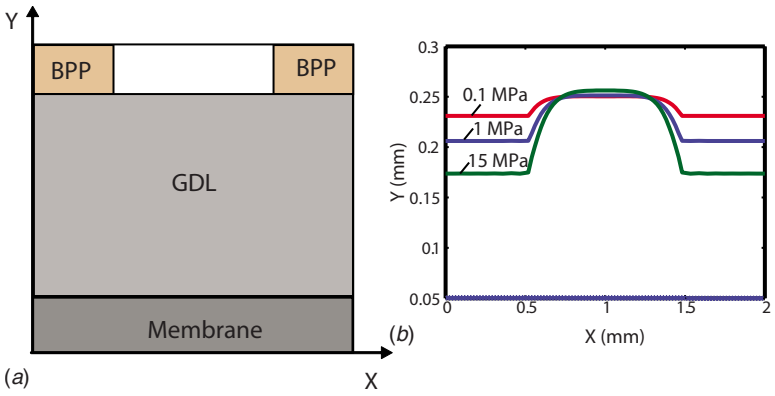

Fig. 3 (*a*) Cell geometry before deformation and (*b*) deformed shapes of GDL under assembly pressures 0.1 MPa, 1 MPa, and 15 MPa, respectively

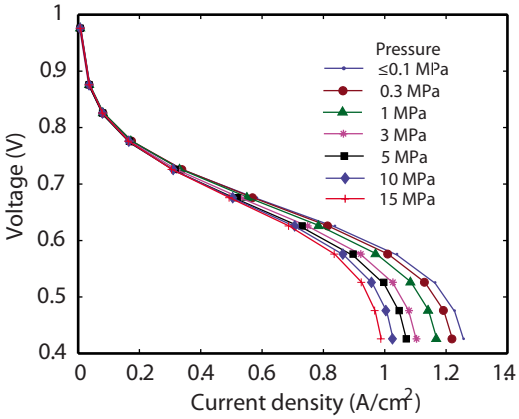

Fig. 5 Assembly pressure effect on PEM fuel cell performance with only mass transfer resistance being considered

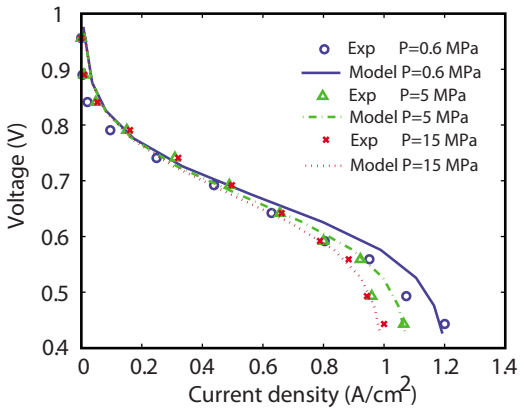

Fig. 7 Polarization curves comparison between the modeling results with the experimental data under different assembly pressures.

Lower porosity obstructs gas transfer in the GDL, which is the dominant reason for the assembly pressure effects on mass transfer resistance. For the same surface overpotential η, the current density increases with porosity. Again, this is obviously due to the fact that a larger porosity in the GDL leads to a larger consumption of oxygen in the catalyst layer, from which a larger current density is generated. Moreover, a change in the porosity of the GDL has virtually less influence on the voltage level when the current density is at a medium or low value. It has a significant effect, however, on the polarization curve when the current density is close to the limiting value. This result is consistent with the fact that the voltage curve in the regime close to the limiting current density is governed by the mass transfer resistance, as stated in previous studies [24].

In this model, the reduction in channel flow area and GDL thickness has little impact on the overall performance. However, if the initial thickness of the GDL is larger, or the channel depth is smaller, this effect could be more prominent.

3.3 Assembly Pressure Effects on Electrical Contact Resistance. The surface roughness parameters of the same type of BPP (POCO AXF-5QCF) used in single cell tests [12] are measured to estimate the electrical contact resistance in the cell, which is then integrated into the performance model results. The surface roughness parameters obtained from the average values of several scans are peak density $D_{peak}=150/\text{mm}$, mean asperity summit radius $R_1=3.26\ \mu\text{m}$, and variance of the summit height distribution $\sigma_s=0.728\ \mu\text{m}$. The GDL material properties and the structure used in the simulation are based on the characteristics of Toray carbon fiber paper. The contact resistance change with assembly pressure, which is applied at the top of BPP, is shown in Fig. 6.

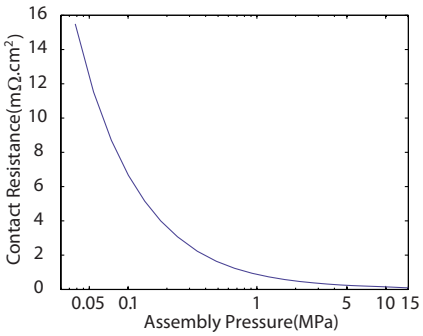

Fig. 6 Simulated contact resistance versus assembly pressure

4 Model Validation and Discussion

4.1 Validation. To validate the numerical model presented in Sec. 3, the comprehensive model results are compared with the experimental data from Ref. [12] for a cell with a single serpentine channel and the same geometry and operation parameters.

Figure 7 compares the simulated voltage curves with the measured ones at 0.6 MPa, 5 MPa, and 15 MPa assembly pressures. The simulated curves are generally in good agreement with the experimental data. However, the simulated cell current densities in the high current density region are slightly higher than the experimental values. This discrepancy is a common feature of single-phase models where the effect of water flooding in the cathode at high current density is not accounted for. More current is produced under the channel area than under the land area because of the reduced oxygen diffusion in the compressed region. Thus, water flooding under the channel area is more severe than under the land. This makes the GDL porosity uneven, sometimes considerably. In this model, the porosity is assumed to be the average value throughout the GDL in every assembly pressure, which could already reflect the overall effect of assembly pressure, with water flooding taken into account, on GDL porosity. Ideally, if the porosity is allowed to decrease in the model in proportion to cell current, to account for enhanced generation of water in the GDL, as well as change with cell dimensions due to compression, the model could predict the performance more accurately.

4.2 Assembly Pressure Effects on the Overall PEM Fuel Cell Performance. Upon obtaining assembly pressure effects on mass transfer resistance and contact resistance above, the overall PEM fuel cell performance can be evaluated, as shown in Fig. 8.

From Fig. 8, the fuel cell performance decreases with increasing compression in most of the assembly pressure regions. However, an optimum assembly pressure exists within the lower-pressure region. This optimal value is the result of the competing effects of contact resistance and mass transfer resistance. When the assembly pressure is very low, contact resistance could be high and reverse the effect of low mass transfer resistance. Obviously, an assembly pressure near this optimum value is preferred. Furthermore, if surface parameters of the BPP change, especially when the surface standard deviation becomes larger, the contact resistance tends to be higher. The optimum assembly pressure could then shift to a higher level, which can be achieved in practical assembly processes.

In addition to the overall polarization curve changes with assembly pressure, local current density distribution at the catalyst layer surface also differs, as presented in Fig. 9. For a lower value of assembly pressure (0.6 MPa), a much higher current density is generated under the channel area. This is because a compressed

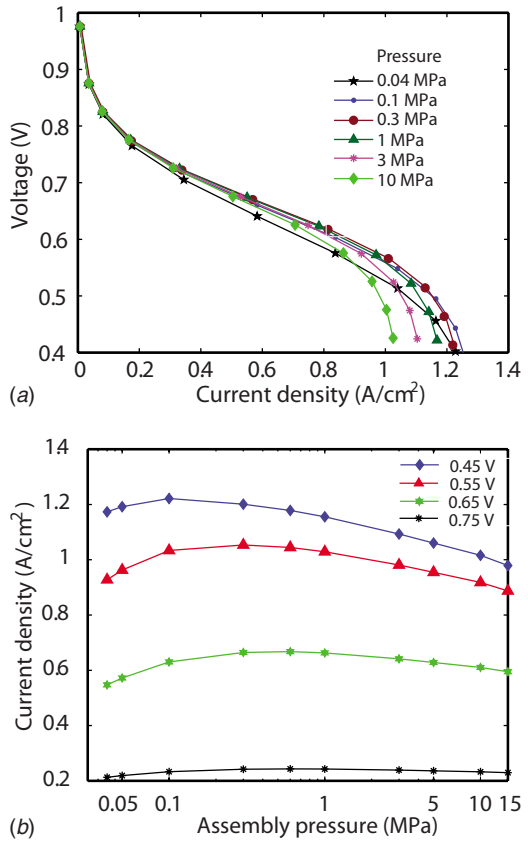

Fig. 8 Effect of assembly pressure on overall fuel cell performance: (*a*) polarization curves at different assembly pressures and (*b*) current density versus assembly pressure at different cell voltages

GDL increases the resistance of oxygen diffusion into the region under the land, resulting in a lower local oxygen concentration. Moreover, the current density distribution becomes slightly more nonuniform as the assembly pressure increases because of the reduced oxygen diffusion in compressed region. Higher assembly pressure (15 MPa) leads to smaller porosity, which imposes more impedance to gas transfer. Thus the current density generated under the land area is less and has more variation in its distribution.

Figure 10 shows the O_2 mass distribution of the cross section of the GDL at the channel outlet for the same overpotential under 0.6 MPa and 15 MPa assembly pressures. The O_2 mass fraction decreases noticeably inside the GDL, particularly under the land area. This effect is more pronounced for high assembly pressure conditions, where O_2 mass fraction still remains very low regardless of the high O_2 mass fraction gradient.

5 Conclusions

In order to study the effects of assembly pressure on the performance of PEM fuel cells mathematically, a multiphysics model was developed to simulate the entire process including the effects of mechanical deformation, mass transfer resistance, and electrical contact resistance. After obtaining GDL deformation numerically, a 3D model was built to predict the mass transfer of gas based on the deformed geometry and associated parameters. Next, an overall PEM fuel cell performance model was proposed by integrating a mass transfer resistance model and a microscale electrical contact resistance model previously developed by the authors. The model results were in good agreement with available experimental data from literature.

It has been observed that assembly pressure has significant effects on PEM fuel cell performance. Generally, high assembly pressure increases mass transfer resistance. Current density decreases dramatically with an increase in assembly pressure. However, by incorporating the competing effect of electrical contact resistance, the overall performance first increases and then decreases with the increase in assembly pressure. There exists an

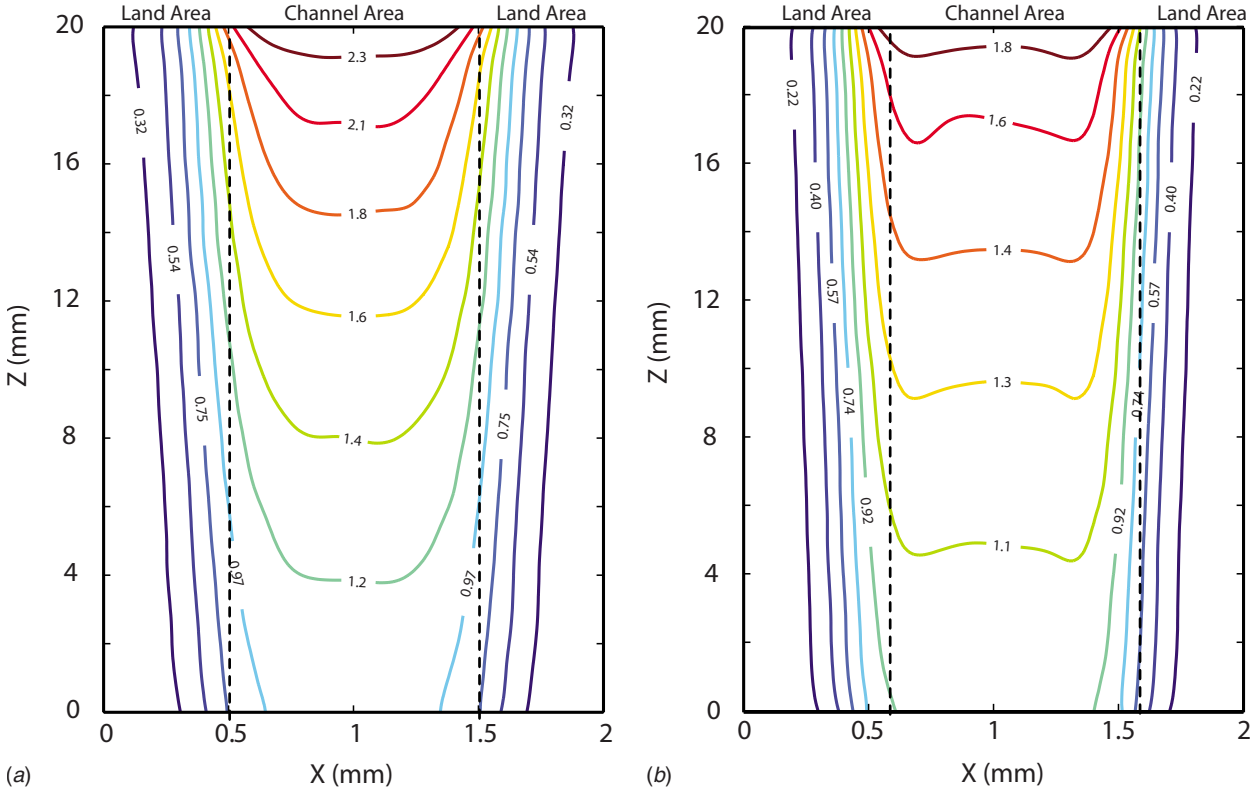

Fig. 9 Contours of the current density at 0.58 V cell voltage and assembly pressures of (*a*) 0.6 MPa and (*b*) 15 MPa

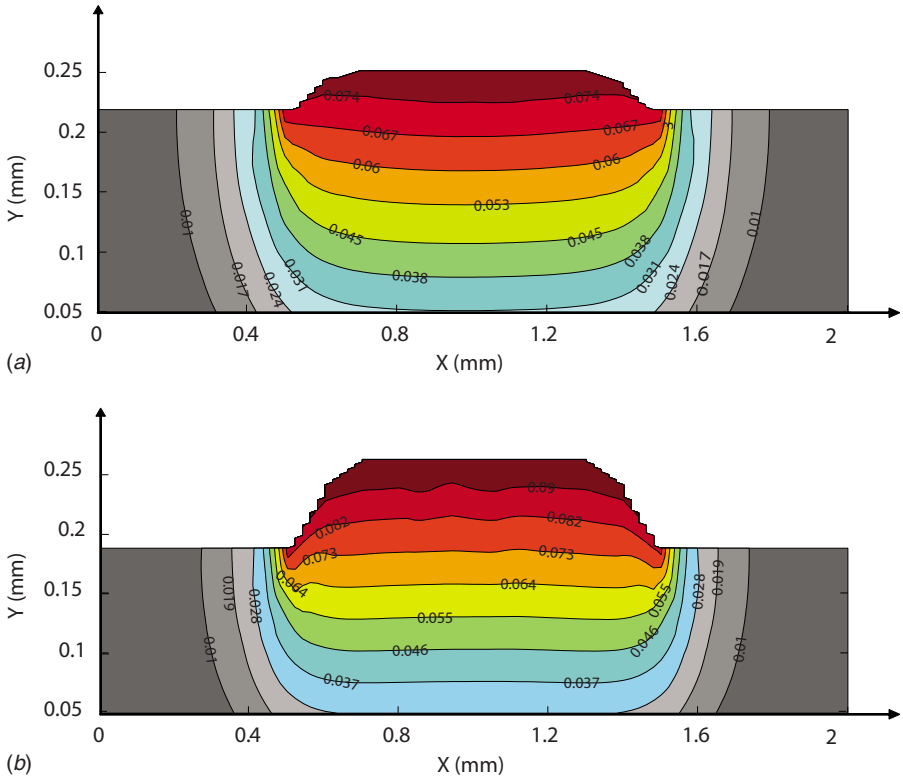

Fig. 10 O_2 mass faction in GDL at channel outlet at assembly pressures (*a*) 0.6 MPa and (*b*) 15 MPa

optimum assembly pressure, in the lower-pressure region, at which fuel cell performance is maximized. Finally, current density distribution and O_2 mass fraction distribution were also discussed. This study could provide guidance for potential improvements in the PEM fuel cell design and assembly.

Acknowledgment

The authors would like to thank Professor Hongtan Liu and Jiabin Ge from the University of Miami for providing the experimental for model validation.

References

[1] Springer, T. E., Zawodzinski, T. A., and Gottesfeld, S., 1991, "Polymer Electrolyte Fuel Cell Model," J. Electrochem. Soc., **138**(8), pp. 2334–2342.
[2] Bernardi, D. M., and Verbrugge, M. W., 1991, "Mathematical Model of a Gas Diffusion Electrode Bonded to a Polymer Electrolyte," AIChE J., **37**(8), pp. 1151–1162.
[3] Fuller, T. F., and Newman, J., 1993, "Water and Thermal Management in Solid Polymer Electrolyte Fuel Cells," J. Electrochem. Soc., **140**(5), pp. 1218–1225.
[4] Nguyen, T. V., and White, R. E., 1993, "A Water and Heat Management Model for Proton Exchange Membrane Fuel Cells," J. Electrochem. Soc., **140**(8), pp. 2178–2186.
[5] Chi, P. H., Weng, F. B., Su, A., and Chan, S. H., 2006, "Numerical Modeling of Proton Exchange Membrane Fuel Cell With Considering Thermal and Relative Humidity Effects on the Cell Performance," ASME J. Fuel Cell Sci. Technol., **3**, pp. 292–302.
[6] Berning, T., Lu, D. M., and Djilali, N., 2002, "Three-Dimensional Computational Analysis of Transport Phenomena in a PEM Fuel Cell," J. Power Sources, **106**(1–2), pp. 284–294.
[7] Berning, T., and Djilali, N., 2003, "Three-Dimensional Computational Analysis of Transport Phenomena in a PEM Fuel Cell—A Parametric Study," J. Power Sources, **124**(2), pp. 440–452.
[8] Lai, Y. H., Miler, D. P., Ji, C., and Trabold, T. A., 2004, "Stack Compression of PEM Fuel Cells," *Proceedings of Fuel Cell 2004: The Second International Conference on Fuel Cell Science, Engineering and Technology*, Rochester, NY, Jun. 14–16.
[9] Lee, W. K., Ho, C. H., Van Zee, J. W., and Murthy, M., 1999, "The Effects of Compression and Gas Diffusion Layers on the Performance of a PEM Fuel Cell," J. Power Sources, **84**(1), pp. 45–51.
[10] Lee, S. J., Hsu, C. D., and Huang, C. H., 2005, "Analyses of the Fuel Cell Stack Assembly Pressure," J. Power Sources, **145**(2), pp. 353–361.
[11] Chu, H. S., Yeh, C., and Chen, F., 2003, "Effects of Porosity Change of Gas Diffuser on Performance of Proton Exchange Membrane Fuel Cell," J. Power Sources, **123**(1), pp. 1–9.
[12] Ge, J., Higier, A., and Liu, H., 2006, "Effect of Gas Diffusion Layer Compression on PEM Fuel Cell Performance," J. Power Sources, **159**(2), pp. 922–927.
[13] Bazylak, A., Sinton, D., Liu, Z. S., and Djilali, N., 2007, "Effect of Compression on Liquid Water Transport and Microstructure of PEMFC Gas Diffusion Layers," J. Power Sources, **163**, pp. 784–792.
[14] Chang, W. R., Hwang, J. J., Weng, F. B., and Chan, S. H., 2007, "Effect of Clamping Pressure on the Performance of a PEM Fuel Cell," J. Power Sources, **166**, pp. 149–154.
[15] Nitta, I., Hottinen, T., Himanen, O., and Mikkola, M., 2007, "Inhomogeneous Compression of PEMFC Gas Diffusion Layer," J. Power Sources, **171**, pp. 26–36.
[16] Zhou, P., and Wu, C. W., 2007, "Numerical Study on the Compression Effect of Gas Diffusion Layer on PEMFC Performance," J. Power Sources, **170**, pp. 93–100.
[17] Springer, T. E., Wilson, M. S., and Gottesfeld, S., 1993, "Modeling and Experimental Diagnostics in Polymer Electrolyte Fuel Cells," J. Electrochem. Soc., **140**, pp. 3513–3526.
[18] Inoue, G., Matsukuma, Y., and Minemoto, M., 2006, "Effect of Gas Channel Depth on Current Density Distribution of Polymer Electrolyte Fuel Cell by Numerical Analysis Including Gas Flow Through Gas Diffusion Layer," J. Power Sources, **157**, pp. 136–152.
[19] Mathias, M., Roth, J., Fleming, J., and Lehnert, W., 2003, *Handbook of Fuel Cells—Fundamentals, Technology and Applications*, Vol. 3, W. Vielstich, A. Lamm, H. A. Gasteiger, eds., Wiley, New York, pp. 13.
[20] Cussler, E. L., 1984, *Diffusion-Mass Transfer in Fluid Systems*, Cambridge University, Cambridge, UK.
[21] Newman, J. S., 1991, *Electrochemical Systems*, Prentice-Hall, Englewood Cliffs, NJ, Chap. 1.
[22] Parthasarathy, A., Srinivasan, S., and Appleby, A. J., 1992, "Temperature Dependence of the Electrode Linetics of Oxygen Reduction at the Platinum/Nafion Interface—A Microelectrode Investigation," J. Electrochem. Soc., **139**(9), pp. 2530–2537.
[23] Zhou, Y., Lin, G., Shih, A. J., and Hu, S. J., 2007, "A Micro-Scale Model for Predicting Contact Resistance Between Bipolar Plate and Gas Diffusion Layer in PEM Fuel Cells," J. Power Sources, **163**(2), pp. 777–783.
[24] Hoogers, G., 2003, *Fuel Cell Technology Handbook*, CRC, Boca Raton, FL, Chap. 4.